fibers

MDPI

Article

Rehabilitation and Strengthening of Damaged Reinforced Concrete Beams Using Carbon Fiber-Reinforced Polymer Laminates and High-Strength Concrete Integrating Recycled Tire Steel Fiber

Hasan A. Alasmari [1], Ibrahim A. Sharaky [1], Ahmed S. Elamary [1] and Ayman El-Zohairy [2,*]

[1] Civil Engineering Department, College of Engineering, Taif University, P.O. Box 11099, Taif 21944, Saudi Arabia; h.alasmari@tu.edu.sa (H.A.A.); i.sharaky@tu.edu.sa (I.A.S.); a.elamary@tu.edu.sa (A.S.E.)
[2] Department of Engineering and Technology, East Texas A&M University, Commerce, TX 75429, USA
* Correspondence: ayman.elzohairy@tamuc.edu; Tel.: +1-903-886-5474

Abstract: Currently, millions of tires are consumed annually, which necessitates the efficient disposal of these quantities of spent tires and the development of means to convert them into useful materials. This research deals with the effect of adding the steel fibers extracted from used car tires (RSFs) to incorporate them as concrete components to obtain high-strength concrete (HSC). The HSC was used in this paper to strengthen the pre-damaged beams by jacking. In the first phase, twelve beams were subjected to an overload equal to 80% of their total expected bearing capacity to obtain damaged RC beams, while one beam was loaded to failure (reference beam, RB0). In the second phase, the damaged beams were strengthened with HSC jacketing integrating RSFs with three contents (0, 0.25, and 0.5%) or by HSC jacking and bonded CFRP laminates to the bottom surface of the jacket. Moreover, the Abaqus finite element (FE) program was implemented to simulate the upgraded damaged beams. The result ensured enhanced HSC compressive and tensile strengths by 11.6–14.4% and 11.6–20.9% as the RSF % increased from 0 to 0.25 and 0.5%, respectively. Using the HSC jacket with 0, 0.25, and 0.5% RSF to strengthen the RC-damaged beams increased the load capacity by 8.8, 14.5, and 20.1%, respectively compared to RB0. Furthermore, strengthening the damaged RC beams with both HSC jacket and CFRP laminates enhanced their load capacity by 41.9, 45.5, and 50.3% as the HSC integrated 0, 0.25, and 0.5% RSF, respectively, compared to RB0. Finally, the FE model could reveal several aspects related to the behavior of the damaged beams strengthened with jackets and CFRP laminates and the interaction between the different beam components.

Keywords: recycled steel fibers; high-strength concrete; damaged beam; CFRP laminate; HSC jacket

check for updates

Academic Editor: Luciano Ombres

Received: 25 November 2024
Revised: 22 December 2024
Accepted: 3 January 2025
Published: 15 January 2025

Citation: Alasmari, H.A.; Sharaky, I.A.; Elamary, A.S.; El-Zohairy, A. Rehabilitation and Strengthening of Damaged Reinforced Concrete Beams Using Carbon Fiber-Reinforced Polymer Laminates and High-Strength Concrete Integrating Recycled Tire Steel Fiber. *Fibers* **2025**, *13*, 10. https://doi.org/10.3390/fib13010010

Copyright: © 2025 by the authors. Licensee MDPI, Basel, Switzerland. This article is an open access article distributed under the terms and conditions of the Creative Commons Attribution (CC BY) license (https://creativecommons.org/licenses/by/4.0/).

1. Introduction

Reinforced concrete (RC) structures are subject to deterioration over time, which can lead to significant performance degradation and potentially dangerous consequences [1]. The rehabilitation and strengthening of RC structural components in extant buildings are crucial for prolonging their operational lifespan. Conversely, if such measures are not undertaken, the structure would necessitate demolition and reconstruction. In most cases, the strengthening or repair of structures proves to be a more economical solution compared to the option of demolition and new construction [2]. Structural strengthening demands may emerge from concrete structures that are subject to deterioration over time,

which can lead to significant performance degradation and potentially dangerous consequences [3] and alteration in the utilization of the building with increased load demands. In all circumstances, the load-bearing components necessitate reinforcement to augment their capacities. Previous research has identified numerous rehabilitation solutions tailored to the specific structure and loading conditions based on the extent of structural damage. There are numerous well-known techniques for strengthening RC structures either in shear or flexural performance [4,5], such as near-surface mounted (NSM) [6–13], externally bonded (EB) [14–16], and high-strength concrete layers [17–22]. These methods have been employed recently to enhance the flexural capacity of RC members such as increasing the effective depth by adding concrete to the compression zone, applying glass or carbon fiber-reinforced polymer (FRP) sheets to the tension surface of flexural members, wrapping members with textile fiber-reinforced concrete/mortar jackets, and applying a strain-hardening cementitious composite layer to the tension zone of members [23–26]. Each strengthening technique has its advantages and disadvantages [6,21]. The selection between these methods is influenced by a variety of factors, including economic, social, and environmental considerations and other requirements of the project [27].

The use of concrete layers with different combinations, reinforcement, and strength to upgrade the RC members is now a well-known technique [22,28–32]. In [33], steel fiber-reinforced high-strength lightweight self-compacting concrete (SHLSCC) was utilized to strengthen RC beams, enhancing their bending moment capacities. The study found substantial enhancements in the stiffness of reinforced beams, along with 14–58% increases in peak load capacity when upgraded using 40, 50, and 60 mm layers of SHLSCC. Ultra-high-performance concrete (UHPC) as a strengthening method has experienced substantial growth over the past two decades due to its superior mechanical and durability characteristics compared to normal concrete. Employing UHPC as a repair and/or strengthening material for structural beams can offer several notable advantages, including ease of construction, protection against harsh environmental conditions, enhanced ductility, reduced encasement dimensions, and cost-effectiveness relative to existing repair solutions [34,35].

Fibers play an essential role in enhancing the properties of the ultra-high-performance fiber-reinforced concrete (UHPFRC) [36,37]. With FRP fiber content of 1% or 0.5% (12 mm long) in grid UHPC plates, their flexural capacities increased by 167.76% and 201.08%, respectively, compared with UHPC plates. As the fiber length decreased to 6 mm, the flexural capacity enhancement of FRP grid UHPC plates with 1% or 0.5% content was 105.51% and 101.79% more than those with FRP [36]. Rabehi et al. [38] suggest that the employment of the UHPFRC and concrete jacketing systems can be considered feasible and cost-effective alternatives to conventional repair and strengthening techniques for RC members such as steel and FRP jackets. Furthermore, UHPFRC can be used to strengthen and repair concrete structures, particularly in narrow and hard-to-access locations [18,31,39]. In [31], a parametric study was conducted based on the influence of the height, reinforcement ratio, and fiber orientation of the UHPFRC layer on the capacity of the RC upgraded beam. The research findings indicate that the examined parameters significantly influence the load-displacement behavior of the beam. Moreover, in [1], rectangular non-prestressed RC beams were also rehabilitated utilizing UHRC and tested for flexural and shear performance. The experimental findings indicated that the I-beams upgraded with UHRC layers exhibited substantially enhanced flexural and shear load capacities in comparison to the control I-beams. Conversely, in [29], the performance of self-compacting fiber-reinforced concrete (SCFRC) jackets for upgrading RC beams was investigated. A 60 mm thick traditional RC jacket made of plain concrete with steel bars and 60 and 30 mm thick jackets composed of steel-fiber-RC were used to form strengthening jackets. The reinforcing bar jacket attained the greatest flexural enhancement. Conversely, Folino et al. [30]

examined the shear strengthening of existing RC beams using the established concrete jacketing technique and RC beam strengthening using jackets fabricated with various jacket widths, concrete jacket types, and surface preparation methods. The findings indicate that the investigated high-performance concrete (HPC) was a suitable material for reinforcing existing beams requiring thinner concrete jackets compared to the use of standard concrete.

Another approach to RC strengthening, the utilization of carbon FRP (CFRP) has emerged as an increasingly favored technique for strengthening damaged RC structures. This approach strengthens RC structures through the external bonding of CFRP laminates to become a prevalent retrofit method compared to other strengthening techniques [13,40]. The CFRP advantages make it an effective material in improving the flexural and shear performance of concrete members. Numerous existing RC members have been observed to exhibit deficiencies in shear capacity, necessitating remedial interventions. These deficiencies can arise due to various factors, including inadequate shear reinforcement, diminished steel cross-sectional area resulting from corrosion, increased service demands, and construction flaws. In such circumstances, CFRP strengthening offers an effective solution [41].

The availability of huge numbers of old tires that cause several environmental impacts (EI) encourages using the components of these old tires to produce sustainable concrete [42,43]. Several companies around the world use these old tires to produce crumb rubber and RSFs to be used as sustainable materials in several applications. Previous research has highlighted the inadequate investigation of recycled steel fibers (RSFs) in varying proportions within HSC concrete mixtures specifically formulated for 25 mm jacketing layers. Furthermore, there has been a scarcity of comprehensive studies on jacketing systems that utilize CFRP as an externally bonded reinforcement for lower beam surfaces which are intended to confine rehabilitated beams that have experienced damage. Consequently, this study aimed to evaluate the effectiveness of this composite jacketing system in the rehabilitation of damaged beams. The rehabilitation approach involved externally strengthening the compromised beams through the application of a single layer of CFRP laminates, which were employed as a form of partial external bonding. The RSF content on the efficiency of the concrete jacket was also studied. The original RC beams were subjected to flexural loads of about 80% of their ultimate capacity to form damaged beams. The damaged beams were strengthened with the previously proposed system and loaded to failure. The load-bearing capacity, deformation, ductility, and failure mechanisms were measured, observed, and contrasted. It is anticipated that this research endeavor aims to offer a novel contribution to the sustainability of environmentally friendly concrete.

2. Experimental Program

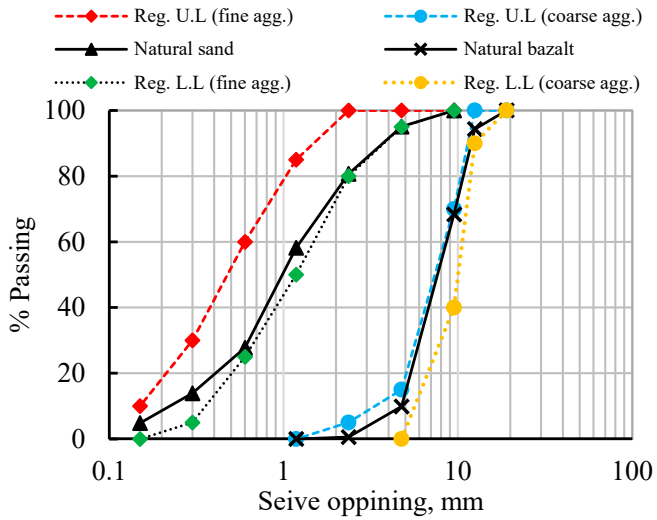
2.1. Materials

The mix design of self-compacting concrete (SCC) used to cast reinforced concrete beam specimens was conducted by Al Jazer Industry Concrete company as shown in Table 1. Crushed stone aggregates with a maximum nominal size of 12.5 mm and natural sand with a specified fineness modulus of 3.0 were utilized as the coarse and fine aggregate concrete components, respectively, and the aggregate grading is shown in Figure 1a. All concrete mixtures were prepared using Super Portland Pozzolanic Cement with a compressive strength of 52.5 N. To improve the workability of the concrete, a superplasticizer (SP, Conplast SP430) with a specific gravity of 1.06 was added to the mixture. It increases the material's overall strength by approximately 20–60% while also improving the durability of the concrete during its service life. The designed mix ratio aimed to achieve a specified compressive strength ranging from 35 to 40 MPa after a curing period of 28 days. Silica fume serves as a component in ultra-high-performance concrete (UHPC), with its inclusion limited to a maximum of 6% because it influences the rheological characteristics of the

UHPC. Furthermore, it has been observed that the compressive strength of UHPC diminishes when the silica fume content surpasses 10% [44]. Incorporating sodium naphthalene sulfonate in the concrete mixture enhances its workability [44]. Tire-derived recycled steel fibers (RSFs) were procured from a local supplier in the Kingdom of Saudi Arabia (Kenzy Rubber Factory). RSF was utilized as the recycled steel fiber reinforcement for M2 and M3. These fibers exhibited a straight configuration, with lengths ranging from 30 to 60 mm and diameters between 0.2 and 0.3 mm as shown in Figure 1b. The specific gravity of the recycled steel bead wires was determined experimentally to be 2.08. According to the supplier's data, the recycled steel bead wires had a strength of 2140 MPa. The HSC was categorized into three groups based on the RSF proportion (0%, 0.25%, and 0.5%; Table 2). The produced HPC was SCC and was used to cast the concrete jacket to strengthen the damaged RC beams. According to BS EN 12390-22009 [45], the compressive strength was tested using three cube samples for each mix after 28 curing days. The splitting–tensile strength test was carried out according to the ASTM C39-05 [46] standards. Three cylinders of 300 mm height and 150 mm diameter for each mixture were tested.

Table 1. Mix proportion for the concrete of the RC beams (1 m^3).

Mix ID	W/C (-)	Natural Sand (kg)	Natural Basalt (kg)		Admixture		Water (kg)	Cement (kg)
			3/4″ Gravel	3/8″ Gravel	RPC7	SP33 ES		
M0	0.4	856	585	353	0.50	1.00	185	450



(**a**) Sieve analysis of sand and basalt



(**b**) RSF



(**c**) CFRP laminates

Figure 1. Characteristics of aggregates, RSF, and CFRP laminates.

Table 2. Mix proportion for the HPC (1 m^3).

Mix ID	W/C (-)	Sand kg	Water kg	Cement kg	SF kg	RFs %	RFs kg	SP430 kg
M1						0	0	
M2	0.2	887	200	1000	60	0.25	5.21	60
M3						0.5	10.42	

The beams' main reinforcement, addressing compressive and tensile forces, consisted of steel bars with a diameter of 12 mm. These bars displayed a yield strength of 460 MPa, an ultimate strength of 610 MPa, and a Young's modulus of 200 GPa. Furthermore, the stirrups were constructed from 8 mm diameter steel bars, which exhibited a yield strength of 560 MPa and an ultimate strength of 620. The CFRP laminates were utilized as external reinforcement for the damaged RC beams in conjunction with the HSC jacket. The CFRP laminates have a thickness of 0.239 mm, as depicted in Figure 1. Table 3 presents a summary of the properties of the CFRP laminates. The adhesion of the CFRP to the RC beams was facilitated through the use of epoxy resin, the specifications of which are outlined in Table 3.

Table 3. The properties of the CFRP laminates and epoxy (supplier data sheet).

CFRP Laminates		**Epoxy Resin**	
Property	Value	Property	Value
Fiber Area Weight, g/m^2	530	Specific Gravity	1.1
Ultimate Elongation	2.1%	Pot Life at 20o C, mins	~60
Fiber Strength, MPa	>4900	Shear Adhesion Strength, MPa	>14
Fiber Young's Modulus, GPa	>230	Compressive Strength, MPa	>170
Tensile Strength, MPa	3550	Compressive Young's Modulus, GPa	>2.5
Tensile Young's Modulus, MPa	235×10^3	Flexural Strength, MPa	>120
		Tensile Strength, MPa	>37

2.2. Preparation of Beams

Thirteen reinforced concrete (RC) beams with a cross-section of 150 x 200 mm and a length of 1200 mm were fabricated and experimentally investigated (Figure 2). The beams were longitudinally reinforced with four steel bars, each with a diameter of 12 mm, where two bars were placed in tension and the other two in compression. Shear reinforcement comprised twelve stirrups, each 8 mm in diameter, uniformly distributed along the beam's length, as depicted in Figure 3. The reinforced concrete beams were fabricated using a conventional concrete mixture (M0). A total of twelve beams were subjected to flexural testing under a four-point loading arrangement until they reached approximately 80% of their ultimate load capacity, while one beam was tested to failure. The first beam (CB) was loaded to failure, and the cracking behavior was monitored. The authors decided to choose the load-caused cracking of the beams with lengths exceeding half of the beam's height, so the 80% overload was used to load the beams to cause cracking. A similar damage technique was also reported in [47,48]. The HSC mixtures were utilized to strengthen the damaged beams of the group (G1) through the application of a 25 mm thick jacket, as depicted in Figure 4. The dimensions and specifications of the beams following the application of the jacket are illustrated in Figure 5. In the case of group G2, in addition to the implementation of the HSC jacket, EB CFRP laminates were affixed externally by applying a single layer to the bottom surface of the beam (see Figure 4g). The repaired damaged beams were tested after curing the HSC jacket for 28 days. The test specimen beams were categorized into seven experimental groups based on the investigated variables. The tested variables used the HSC strength and strengthening method. The beams tested

at approximately 80% of their ultimate load-carrying capacity and the CB were selected as control specimens to see the effect of repairing methods. In the group G1, two deteriorated RC beams (B11 and B12) were rehabilitated using an HSC jacket cast with M1. Furthermore, two compromised reinforced concrete beams, designated as B21 and B22, were subjected to a strengthening procedure involving a jacketing technique with M2. Similarly, these beams were also reinforced using a jacketing application composed of M3. The primary aim of this experimental setup was to investigate the influence of RSF content within the concrete jacket mixtures on the overall performance of the beams. The HSC was cast from self-compacting concrete with fine materials so the mortar in these mixes may close the nearest portions of the cracks and enhance the crack concrete properties and bonding. Consequently, in group G2, six beams were reinforced in a manner alike to those in group G1 but with the additional incorporation of a single layer of EB CFRP laminates. This adjustment was intended to evaluate the synergistic effects of EB CFRP reinforcement alongside the HSC jacket on the structural behavior of the beams. Detailed information regarding the strengthening techniques employed for all beams is presented in Table 4.

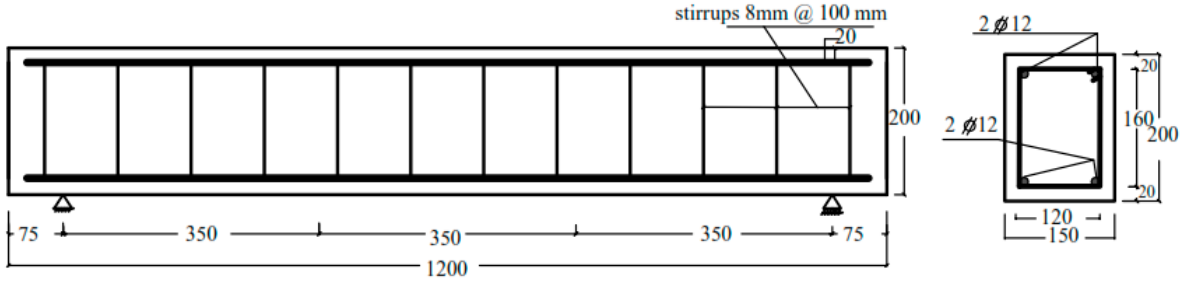
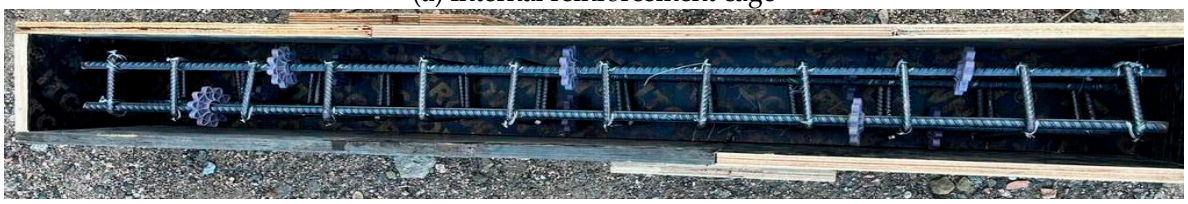


Figure 2. The dimensions and reinforcement of the RC beams.



(**a**) Internal reinforcement cage



(**b**) Installing the reinforcing cage in the mold



(**c**) Casting concrete

Figure 3. *Cont.*



(**d**) Demolding the concrete beams



(**e**) Curing the concrete beams

Figure 3. The preparation of the concrete beams.



(**a**) Adjusting the bottom thickness of the jacket



(**b**) Adjusting the deteriorated beams in the mold



(**c**) Casing the HSC jacket



(**d**) Finishing the concrete jacket



(**e**) Demolding the strengthened concrete beam



(**f**) Curing the concrete jacket

Figure 4. *Cont.*



(**g**) Bonding the CFRP sheets for the specific beams

Figure 4. Strengthening the concrete beams with jacket or CFRP and jacket.

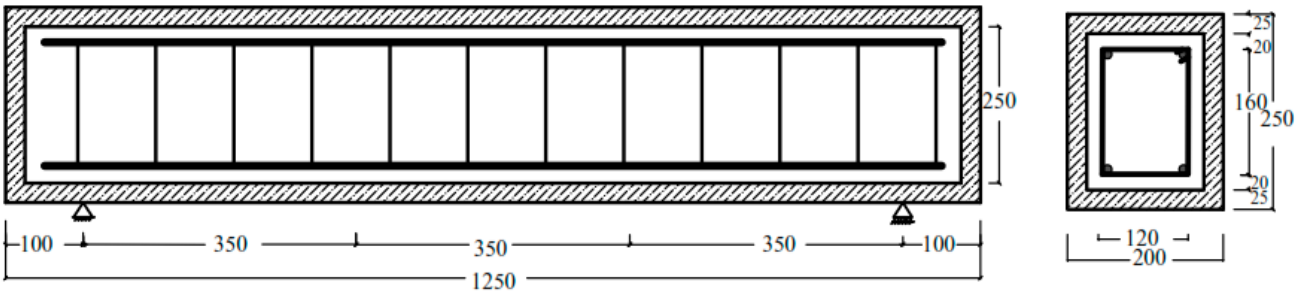


Figure 5. The details and dimensions of the deteriorated beams after applying the HSC jacket.

Table 4. Configuration of the tested beams.

Group ID	Beam ID	HSC Mix	Strengthening Scheme	Test Variables
CB	RB0	Non	Non	Control beam (CB)
G1	RB11 RB12	M1	HSC jacket	HSC strength
	RB21 RB22	M2		
	RB31 RB32	M3		
G2	RB41 RB42	M1	HSC jacket + CFRP	HSC Strength and CFRP
	RB51 RB52	M2		
	RB61 RB62	M3		

2.3. Experimental Set-Up and Instrumentation

Four-point bending tests were conducted on all evaluated beams before and after rehabilitation, with a shear span of 350 mm and beam span of 1050 mm. A loading frame equipped with a 2000 kN hydraulic jack was utilized to automatically apply the load at a displacement rate of 0.6 mm/min (Figure 6). A single linear variable differential transformer was employed to measure the mid-span vertical deflection (LVDT), and data acquisition collection directly connected to a computer was used to record the measured data at a frequency of one data point per second. In the first round, twelve reinforced-concrete (RC) beams were loaded until 80% of their ultimate capacity, at which hairline cracks emerged. The damaged beams were strengthened using HPC jackets or HPC jackets with a CFRP layer. An incremental load was applied to the strengthened beams until the beginning of failure (Figure 6), and the cracks were visually monitored and observed at various load levels. The cracks were identified, marked, photographed, and documented.

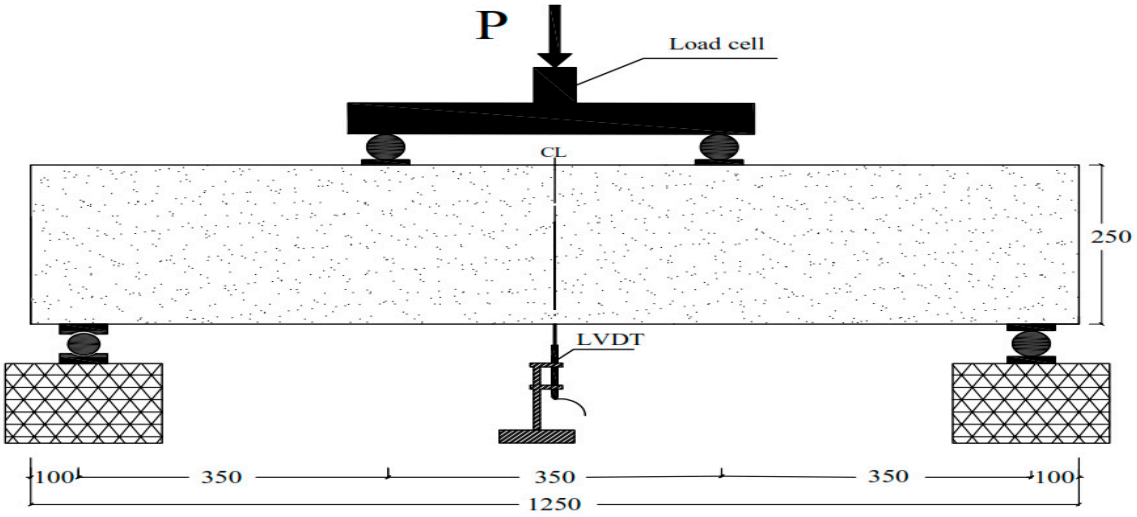


Figure 6. Test set-up and instrumentation of the strengthened damaged RC beams.

3. Results and Discussion

3.1. Concrete Properties

The slump test is a common test for measuring concrete consistency at the site and labs to ensure the specified slump for design specification. In this study, slump values for all mixtures were measured and are listed in Table 5. For the control mix (M0, normal concrete (NC)), the slump measured by the slump cone test was 120 mm. The slump value for the HSC mixes was measured using the slump flow test where the M1 slump was 750 mm. Adding RSF to the concrete mixes (M2 and M3), the slump value decreased with increasing the RSF %. The RSF may withstand the flow of other concrete components, so it reduces the slump. In [49,50], increasing the RSF ratio up to 3% enhanced strength. The slump diminished as the RSF content increased because the RSF has a random geometry that allows the RSFs to entangle with each other and with the coarse aggregate [49]. Also, their small diameters compared to conventional fibers increase the RSF numbers for similar content. The use of 1% RSF may be suitable to achieve both strength and suitable workability.

Table 5. Properties of fresh and hardened concrete mixes with and without fibers.

Mix (ID)	Fibers (%)	Slump (mm)	f_{cu}, (MPa)	$f_{cu,Av.}$ (MPa)	μ_{cu} (%)	f_{tu} (MPa)	f_{tu} (MPa)	μ_{tu} (%)
M0	0.00	130	38.9 40.4 39.5	39.6	-	3.5 3.7 3.6	3.6	-
M1	0.00	750	64.1 66.2 65.2	65.2	-	4.3 4.2 4.4	4.3	-
M2	0.25	700	73.6 72.5 72.4	72.8	111.6	4.9 4.8 4.7	4.8	111.6
M3	0.50	600	76.0 74.1 73.7	74.6	114.4	5.1 5.3 5.2	5.2	120.9

f_{cu} = Compressive strength, f_{tu} = tensile strength, $\mu_{cu} = f_{cu,\,any}/f_{cu,M0} \times 100$, $\mu_{tu} = f_{tu,\,any}/f_{tu,M0} \times 100$.

Incorporating RSF into concrete mixtures has significantly enhanced both compressive and tensile strength characteristics. In a recent study, the control mixture (M0), which lacked RSF, demonstrated compressive and tensile strengths of 39.6 MPa and 3.6 MPa, respectively. In contrast, adding RSF to the mixed design led to notable improvements. Specifically,

the high-strength concrete mixtures (M1, M2, and M3) displayed substantial increases in compressive strength, with values reaching 65.2, 72.8, and 74.6 MPa, respectively. As the RSF percentage increased from 0 to 0.25 and 0.5%, the average compressive strength ($f_{cu,Av.}$) surged by 11.6 and 14.4%, respectively. Concurrently, the tensile strength of the HSC mixes also experienced significant gains. M2 and M3 exhibited tensile strength increases of 11.6, and 20.9%, respectively, when compared to M1. These findings underscore the positive impact of RSF on the mechanical properties of concrete. By reinforcing the concrete matrix with RSF, the RSF bridging cracks could improve load-carrying capacity and durability. This enhanced performance makes RSF-reinforced concrete a promising material for various structural applications, particularly in situations where high strength and toughness are required. The impact of RSF on the improvement of concrete tensile strength was distinctly illustrated through a comparison of the tensile strengths of M1, M2, and M3, emphasizing the enhancement in tensile strength as the RSF increased from 0% to 0.5%. In [49], the RSF enhanced the concrete strength by up to 49.7% compared to concrete with hooked steel fibers, specifically at high temperatures.

3.2. Behavior of Loaded RC Beams Before Strengthening

The data presented in Table 6 provide an extensive analysis of the crack patterns identified in concrete beams subjected to 80% of their expected maximum load capacity during the static testing phase, while the RB0 tested to failure (reference beam). The RB0 beam displayed a significant length of crack lines with 18 mm, a notable width of 0.8 mm, and an inclination angle of 87 degrees. The spacing between these cracks varied considerably, with a minimum distance of 6 mm and a maximum of 14 mm. In contrast, the experimental beams tested to 80% of their expected load capacity showed a significant decrease in both the length and width of the crack lines. The length of cracks was restricted to between 9 and 11, and their widths were considerably smaller, ranging from 0.21 mm to 0.61 mm. Additionally, the inclination angle of these cracks increased to 90 degrees, indicating a more perpendicular alignment to the longitudinal axis of the beam. The spacing between the cracks also expanded, with a minimum of 9 mm and a maximum of 17 mm. For all the tested beams under 80% of their maximum loads and the CB, very narrow flexural cracks appeared at a load ranging between 35 and 37 kN. As the load rose, the number, length, and width of the flexural cracks increased, and cracks in the shear spans started to appear until the load stopped. For the CB, the shear cracks propagated towards the loading points causing shear failure for the beam.

Table 6. Details of cracks in the beams before strengthening.

Group ID	Beam ID	L_c (-)	$L_{c\,av.}$ (mm)	W_c (mm)	$W_{c,av.}$ (mm)	θ (°)	$θ_{av.}$ (°)	$S_{min.}$ (mm)	$S_{min,av.}$ (mm)	S_{max} (mm)	$S_{max,av.}$ (mm)
RB0	CB	18.0	18.0	0.80	0.80	87.0	87.0	6.0	6.0	14.0	14.0
RB1	RB11	10.0	10.0	0.43	0.61	91.0	89.0	7.0	5.0	15.0	17.0
	RB12	10.0		0.79		87.4		4.0		19.0	
RB2	RB21	12.0	10.0	0.22	0.21	90.5	89.0	8.0	6.0	10.0	13.0
	RB22	8.0		0.20		87.5		4		15.0	
RB3	RB31	10.0	10.0	0.71	0.47	68.2	78.0	8	9.0	15.0	17.0
	RB32	9.0		0.23		88.8		10		18.0	
RB4	RB41	7.0	9.0	0.23	0.23	81.2	83.0	6	5.0	21.0	16.0
	RB42	10.0		0.22		85.8		4		10.0	
RB5	RB51	12.0	10.0	0.50	0.32	83.0	88.0	3	9.0	15.0	16.0
	RB52	8.0		0.13		92.3		16		17.0	
RB6	RB61	10.0	11.0	0.25	0.29	90.0	90.0	4	5.0	14.0	14.0
	RB62	12.0		0.33		89.0		6		14.0	

L_c = maximum crack length, $L_{c,av}$ = average crack length, W_c = maximum crack width, $W_{c,av}$.= average crack width, θ = maximum crack inclination angle, $θ_{av.}$= maximum crack inclination angle, S_{min} = minimum crack spacing, $S_{min,av}$ = average minimum crack spacing, S_{max} = maximum crack spacing, and $S_{max,av}$ = average maximum crack spacing.

An overall examination of the results reveals that the beams subjected to a load of 80% of their maximum capacity displayed nearly identical crack patterns and stiffness. This similarity can be attributed to the use of the same concrete mix and identical reinforcement specifications (see Figures 7 and 8). Any differences observed in crack angle, width, and spacing may be linked to the manufacturing processes, including casting and compaction. These beams are scheduled for preparation and reinforcement with HSC jackets and CFRP laminates. The performance of the beams will be evaluated and discussed both before and after the repair in the following sections.

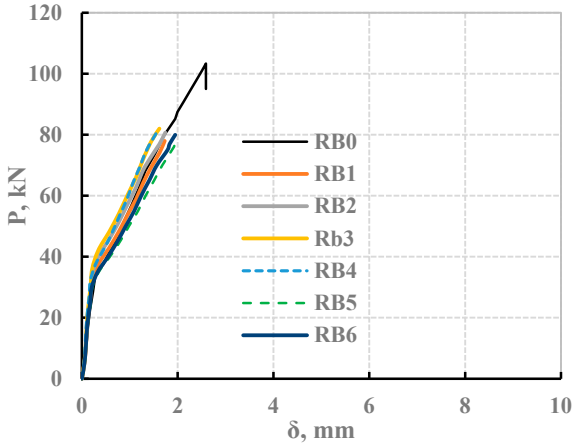


Figure 7. The load deflection of the fully tested RB0 and the partially loaded beams.

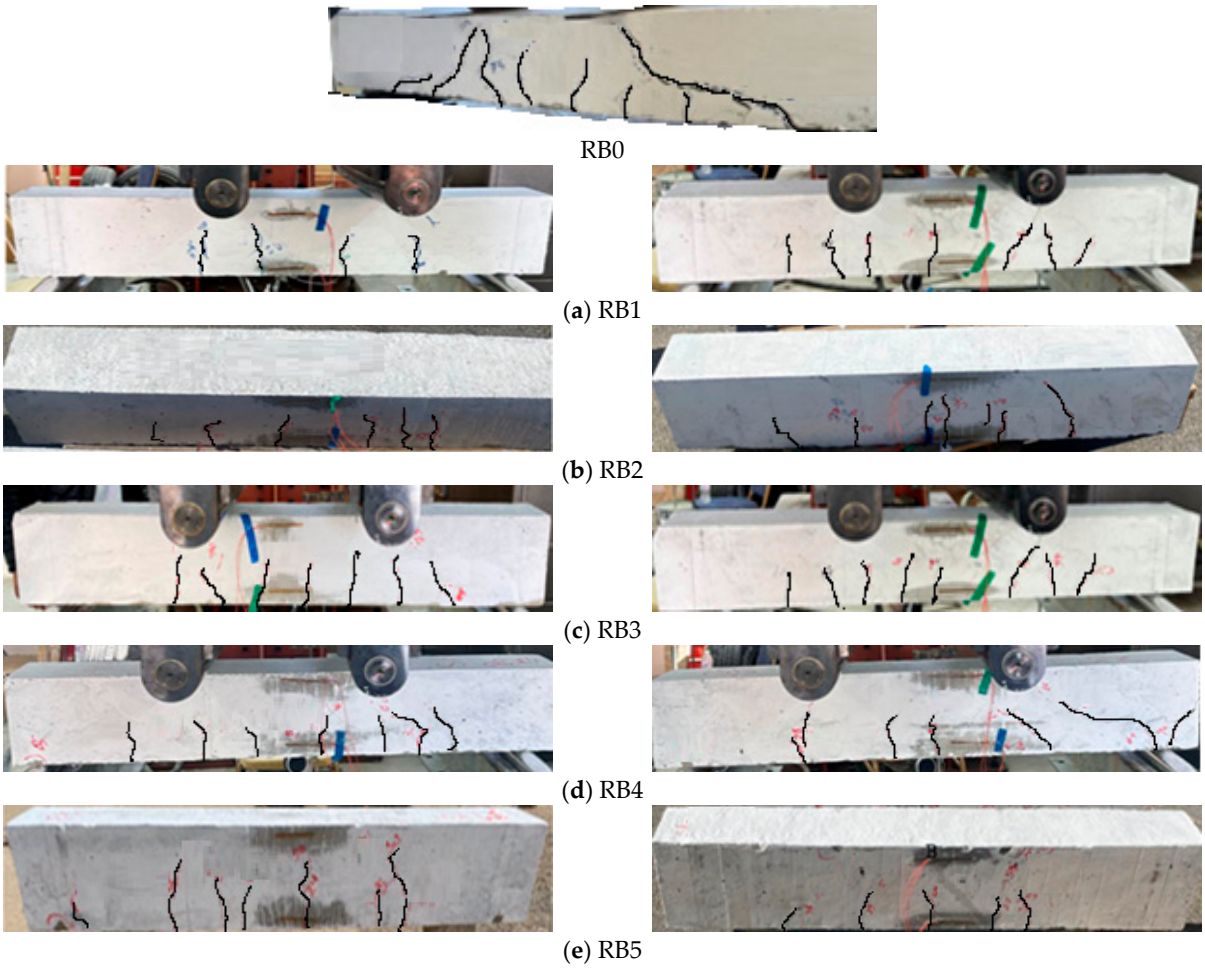


Figure 8. *Cont.*



(**f**) RB6

Figure 8. Cracking of RC beams loaded before strengthening.

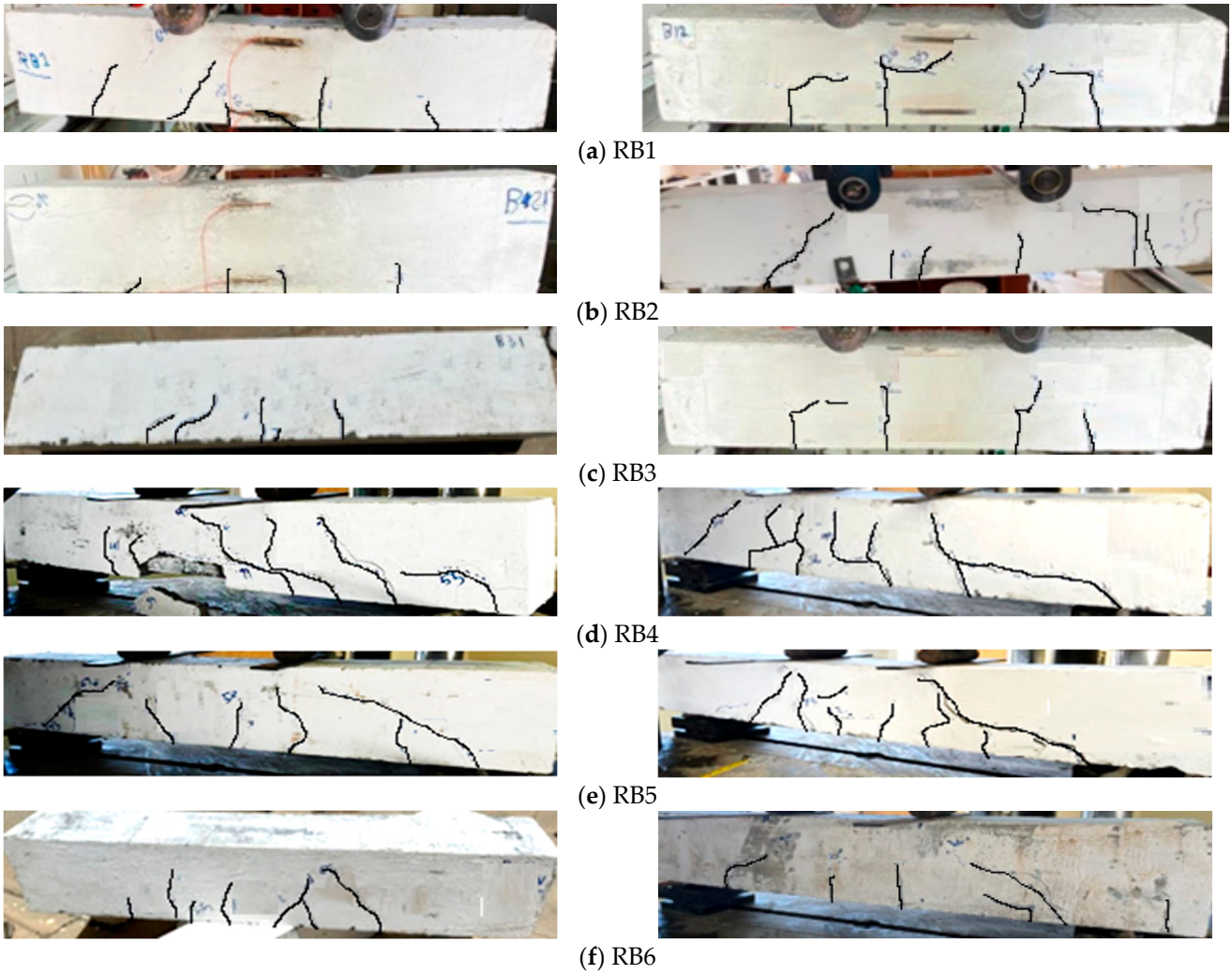
3.3. Results for the Damaged Strengthened RC Beams

3.3.1. Load Capacity and Failure Modes

The damaged beams were strengthened either with an HSC jacket (RB1 to RB3) or with externally bonded CFRP laminate and an HSC jacket (RB4 to RB6) and then tested for failure. The RB0 beam was tested without damaging or strengthening to set a reference beam for comparison. The RB0 beam failed due to shear failure (RH) at a load of 103.1 kN after the spread of cracks along its span. Conversely, the damaged RC beams strengthened with HSC jackets experienced dissimilar load capacities depending mainly on the jacket's HSC strengths. Two beams were tested in each case and their capacities were collected, averaged, and compared as described in Table 7. The yield of the RB1 beam rose by 10.7% while its load capacity increased by 8.8% over that of the RB0 beam (Table 4), but the failure modes were converted from SH to steel yielding (Figure 9a–f). Moreover, the two beams RB2 and RB3 followed the same failure mode of as RB1, but their yielding and ultimate loads increased as the HSC jacket strength increased. The yield load of RB2 and RB3 increased by 17.6 and 22.3%, while their maximum capacities increased by 14.5 and 20.1% over those of RB0, respectively (Table 7). This assured the role of the HSC jacket strengthening for increasing the shear capacity of the RC beam. For beam RB1, the flexural cracks formed in the bottom surface of the HSC jacket and propagated slowly with increasing the applied load until the inside cracked beams. At this time, the cracks propagated rapidly with increasing the deflection related to the load capacity. As the cracks arrived at the level of the steel, the total stiffness of the beam decreased, resulting in steel yielding, and then the load increment decreased, increasing until drop failure occurred due to cracking of the side jacket and high steel deformation (Figure 9a). The two beams RB2 and RB3 follow the same cracking scheme but with slower cracking propagation due to the fiber bridging that arrests the cracks, so these beams showed lower deflections and higher loads capacities. The delaying of flexural crack propagation allowed some shear cracks to appear before failure (Figure 9a,b). The authors expected excessive separation between the concrete jacket to cause the sudden failure and stop the machine from loading.

Bonding the CFRP laminate to the bottom surface of the HSC jacket enhanced the load capacity of the damaged RC beams. The yield capacity of the three beams RB4, RB5, and RB6 rose by 32.5, 36.0, and 38.0% over that of RB0 (Table 7). Consequently, the beam load capacities were also enhanced by 41.9, 45.5, and 50.3%, respectively, over that of the RB0 beam (Table 7). The failure of the beams was SH after Ys (Figure 9, which assured the effect of the CFRP laminate on enhancing the beam flexural capacity, while the HSC strengths increased the beam shear capacity. The CFRP addition to the HSC jacket enhanced the beam capacity by about 21.1 and 5.9% over those without CFRP sheets. The role of the CFRP in delaying the cracking in the three beams RB4-RB6 was obvious from the narrow widths of the flexural cracks. The cracking width of these beams depended on the deformation of the CFRP. After the steel yielded, the drop in the beam stiffness increased its deflection and allowed the shear cracks to form and propagate slowly until arriving at the cracked beam. Afterward, the cracks propagated rapidly with decreasing load capacity and failure. Before yielding, the RSF could play the main role in decreasing the stiffness of the RB5 and RB6 beams. After yielding, this role was decreased due to the high stresses transferred by the sides of the concrete jacket around the shear cracks. Excessive separation between the

concrete jacket was also expected to cause the sudden failure and stop the machine from loading. In [33], substantial enhancements in the stiffness of the reinforced beams were observed, along with 14–58% increases in peak load capacity when upgraded using 40, 50, and 60 mm layers of SHLSCC. The previous results emphasized the contributions of the present method and its sustainability.



(**a**) RB1

(**b**) RB2

(**c**) RB3

(**d**) RB4

(**e**) RB5

(**f**) RB6

Figure 9. Cracking of RC beams loaded after strengthening.

Table 7. The results of the experimentally loaded RC beams.

Beam ID	P_y, kN	R_y %	P_u, kN	R_u %	FM
RB0	95.2	-	103.1	-	SH
RB1-1	103.6		110.8		Ys
RB1-2	107.2		113.6		Ys
RB1	105.4	110.7	112.2	108.8	Ys
RB2-1	113.3		118.9		Ys
RB2-2	110.9		117.1		Ys
RB2	112.1	117.6	118	114.5	Ys
RB3-1	114.6		123.2		Ys
RB3-2	118.2		124.4		Ys
RB3	116.4	122.3	123.8	120.1	Ys
RB4-1	124.9		145.2		Ys, SH
RB4-2	127.2		147.4		Ys, SH

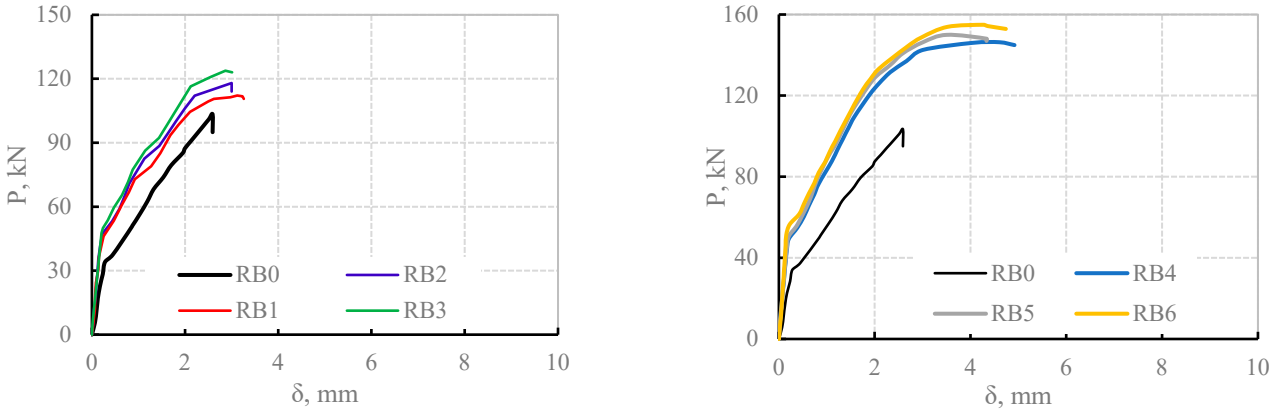
Table 7. *Cont.*

Beam ID	P_y, kN	R_y %	P_u, kN	R_u %	FM
RB4	126.1	132.5	146.3	141.9	Ys, SH
RB5-1	131.2		151.2		Ys, SH
RB5-2	127.8		148.8		Ys, SH
RB5	129.5	136.0	150	145.5	Ys, SH
RB6-1	129.0		152.6		Ys, SH
RB6-2	133.8		157.4		Ys, SH
RB6	131.4	138.0	155	150.3	Ys, SH

$R_y = P_{y,str.}/P_{y,\,RB0}$, $R_y = P_{u,str.}/P_{u,\,RB0}$ and FM = failure mode.

3.3.2. Load–Deflection Curves

The load–deflection (P-δ) of the strengthened damaged RC beams compared to RB0 is summarized in Figure 10. The HSC jacket enhanced the beam's stiffness depending on the HSC strength. Increasing the RSC jacket strength enhanced the stiffness of the damaged strengthened beam (Figure 9a). There was rapid deflection for the beams strengthened with the HSC jacket at different load levels. At these loading levels, the cracks reached the cracked concrete section and might propagate through the weak concrete or fail the HSC jacket-cracked beam bond. The cracks may be shown on the beam surface or hidden inside cracks (Figure 9b–f). Bonding the CFRP laminate to the bottom surface of the HSC jacket enhanced the beam stiffness over beams strengthened with the HSC jacket (Figure 10). The bonding of the CFRP sheets to the bottom surface of the HSC jacket arrested the cracks from propagation in the concrete jacket until steel yielding. Only narrow cracks appeared on the beam surface until the initiation of the shear cracks, which propagated with the load increasing, causing the beam failure. Increasing the HSC properties for the beams with CFRP laminate enhanced both the beam stiffness and the load capacity (Figure 10b). The strengthening of CFRP elements generally enhanced stiffness until the steel yielded, but after yielding, the beam stiffness reduced, so the role of the CFRP was essential in keeping suitable beam stiffness to avoid rapid cracking propagation while increasing beam ductility [6,9].



(**a**) Effect of concrete strength (**b**) Effect of CFRP sheets

Figure 10. The experimental results of the strengthened beams.

3.3.3. Comparison with Other Strengthening Techniques

Due to the availability of RSF as waste materials, its cost is lower than any FRP element that could be used to strengthen RC beams. On the other hand, applying FRP using NSM or EB strengthening methods needed essential preparation and bonding materials, which increased the cost and increased the implementation of the strengthening compared to the HSC jacket with RSF used in this study.

4. FE Modeling

The Abaqus finite element (FE) program was implemented to simulate the upgraded damaged beams.

4.1. Materials Modeling

The properties of normal-strength concrete, HSC, steel, and CFRP laminates were realized. The concrete of the damaged beam was simulated by two concrete strengths (one for the uncracked portion (39 MPa) and the other for the cracked portion (25 MPa). The concrete jacket was simulated with HSC properties in tension and compression. To accomplish this, the elastic modulus Ec and Poisson's ratio (ν) were involved to simulate the elastic responses of all concrete. In contrast, the Concrete Damage Plasticity (CDP) model was involved in simulating their plastic responses and cracking [51]. The CDP model factors were the dilation angle (ψ), the biaxial/uniaxial strength ratio (f_{bo}/f_{co}), the shear ratio (k), and the viscosity (μ). The data of the CDP model representing the compressive and tensile characteristics was calculated from Equations (1)–(5) [52,53]. Two factors (wt and wc) were incorporated to represent the stiffness recovery in tension and compression, respectively. $w_t = 0$ and $w_c = 1$ mean a lack of tension recovery and full compression recovery, respectively, and were considered here for quasi-brittle materials [54]. $d_c = 0$ and $d_c = 1$ represent an undamaged material and a total strength loss of the material, respectively. Equation (1) describes the relationship of concrete stress (σ_c) related to its compressive strength (f'_c), and n is a strength-dependent variable.

$$\frac{\sigma_c}{f'_c} = \frac{n\left(\frac{\varepsilon_c}{\varepsilon'_c}\right)}{n-1+\left(\frac{\varepsilon_c}{\varepsilon'_c}\right)^n} \begin{cases} n = n1, \ \varepsilon_c \le \varepsilon'_c \\ n = n2, \ \varepsilon_c \ge \varepsilon'_c \end{cases} \quad (1)$$

ε_c and ε'_c represent the axial concrete and ultimate tensile strains and were calculated from Equations (2) and (3) [53], while the modulus of elasticity (*Ec*) was obtained from Equation (4):

$$\varepsilon'_c = \left(\frac{f'_c}{E_c}\right)\left(\frac{r}{r-1}\right) \quad (2)$$

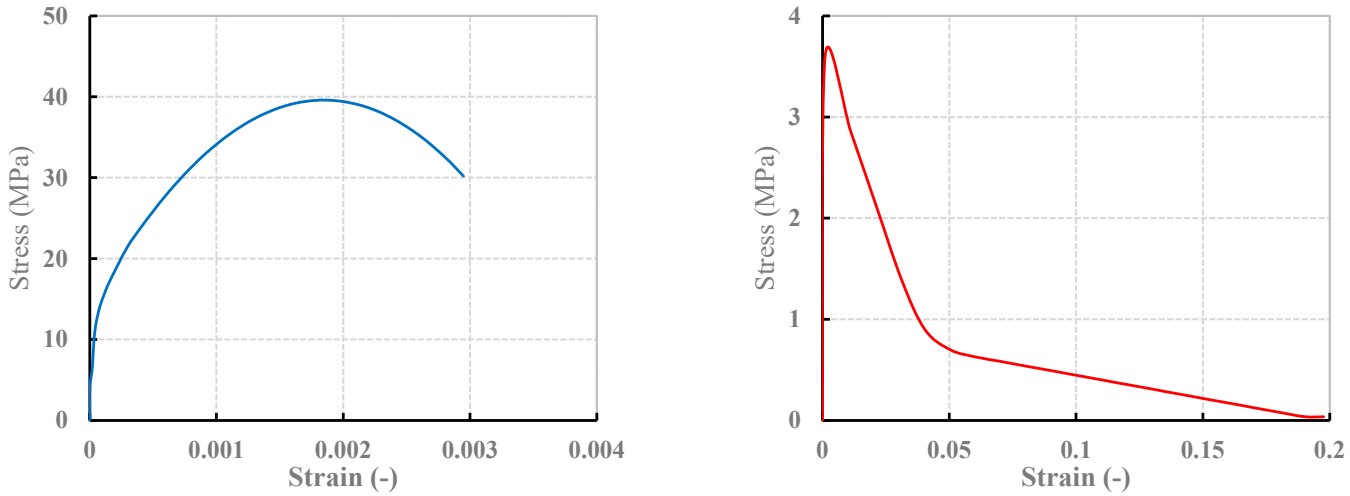
$$r = \left(\frac{f'_c}{17}\right) + (0.8) \quad (3)$$

$$E_c = 3320\left(f'_c\right)^{0.5} + 6900 \quad (4)$$

Equation (5) defines the tensile response [53], and the concrete tensile strength (σ_{tu}) was set to equal 10% of its compressive ones strength.

$$\sigma_t = \sigma_{tu}\left(\frac{\varepsilon_{t0}}{\varepsilon_t}\right)^{0.85} \quad (5)$$

where σ_t is the tensile stress, ε_{t0} is the strain corresponding to σ_{tu}, and ε_t is the tensile strain of the concrete. The CDP model is a suitable macroscale model to simulate concrete with fibers as it allows defining the tensile and compressive stiffness degradation independently. The concrete compressive and tensile σ-ε curves are shown in Figure 11. The concrete model was also set to simulate the response of the bonding epoxy. The elastic–plastic response was set for steel to simulate the behavior of the internal reinforcing bars and both loading and supporting. The CRRP laminate behavior is linear up to failure and is defined in the FE program using their modulus of elasticity and Poisson ratio and the FRP maximum strength.

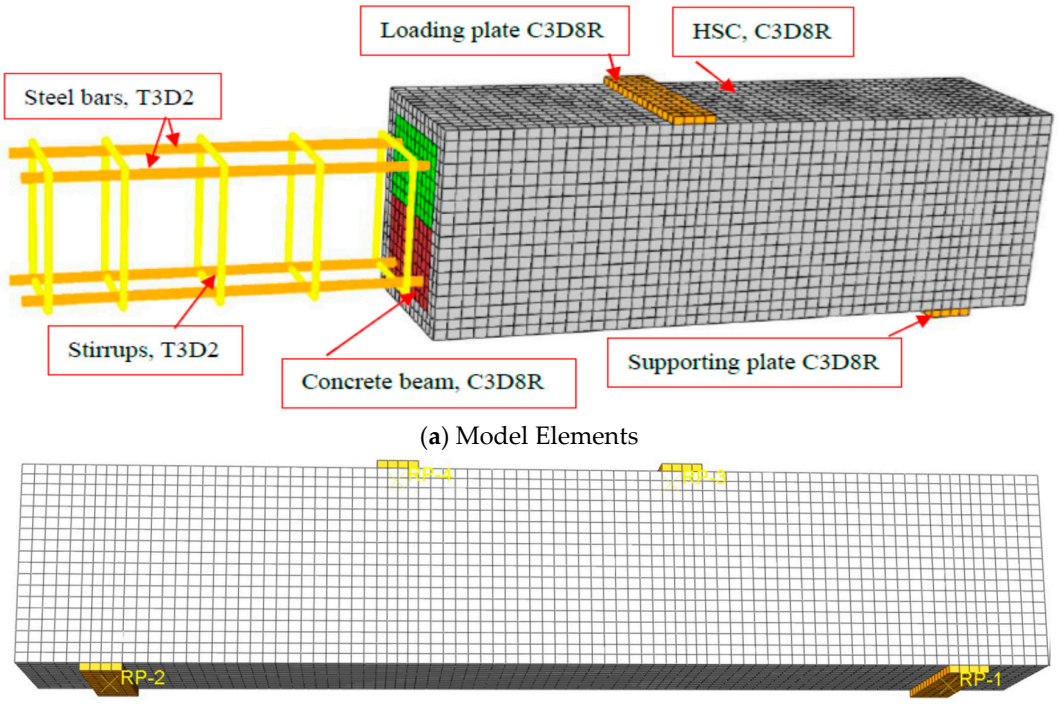


(**a**) Compression behavior (**b**) Tensile behavior

Figure 11. Stress–strain curves of the M_0 concrete.

4.2. Boundary Conditions and Model Characteristics

The set-up, elements, constraints, and mesh of the beams are presented in Figure 12. The concrete of the damaged beams, HSC jacket, loading plates, bonding epoxy, and CFRP laminates were simulated by the eight-node element (C3D8R), Figure 12a, while the internal reinforcing bars were simulated using the truss element (T3D2). The cracked concrete of the damaged beams (the tensile part with about 100 mm thickness) was simulated using reduced concrete properties (compressive strength = 25 MPa), while the top concrete layer was simulated with the concrete properties obtained from the experimental tests (compressive strength = 39 MPa). The embedded region option governed the bonding between the embedded reinforcing bars and the surrounding concrete. As there was no debonding during the experimental tests for the CFRP laminates, the full bond was set to simulate the bonding between the HSC jacket, epoxy, and CFRP laminate. The supports of the beam were tied by rigid body constraints with reference points to apply the beam-supporting constraints (displacements and rotations). To control the loading, the automatic displacement-controlled scheme with a small incremental value (0.1 mm as the maximum) was adopted through the step module. For the reference point (Rf) of one support (roller), the boundary conditions of the beam support were U1 = U2 = U3 = 0 and UR1 = UR2 = UR3 = 0. While the Rf of the other support was restricted as a hinge, the movement and rotations were represented by U1 = U2 = 0 and UR1 = UR2 = UR3 = 0, respectively (Figure 12b). Conversely, a displacement value (about 100 mm) was set to the reference points attached to the loading plates in the Y direction, as shown in Figure 12b. To enhance the FE accuracy, sensitivity analysis with experimental findings was performed to adopt the CDP parameter and mesh of the model. The mesh size of 25 mm (Figure 12b) was designated after performing a sensitivity analysis on several mesh sizes (10, 20, 25, and 30 mm) to achieve minimum solving time at which no significant changes in the results were noticed. The dilation angle (ψ = 35) and viscosity parameter (μ = 0) were also adopted using sensitivity analysis.



(**a**) Model Elements

(**b**) Beam mesh and restraints

Figure 12. Modeling of the simulated beams.

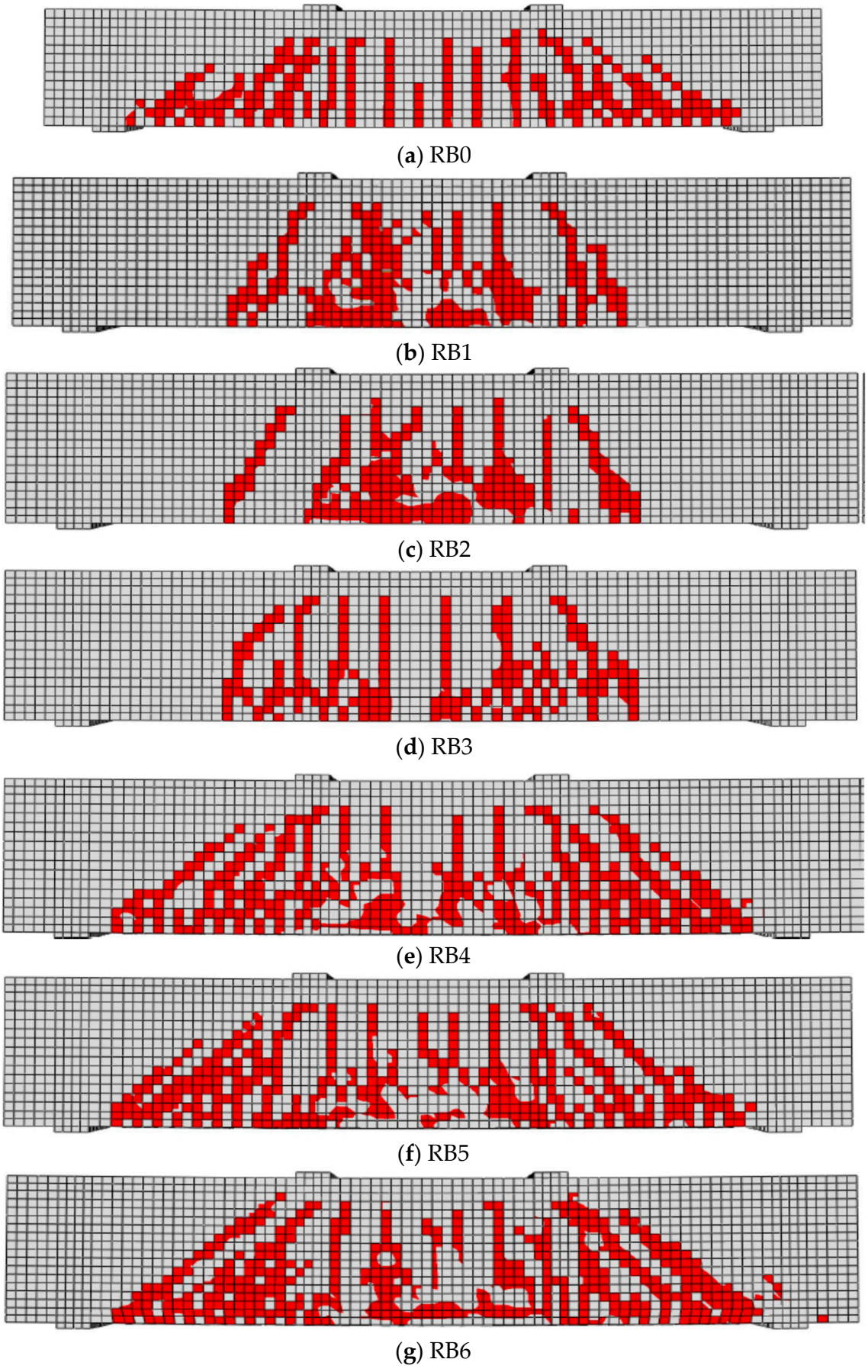
4.3. Verification of the FE Model

To adopt the precision of the FE model, the experimental results were utilized. Detailed companions in terms of yield and maximum load capacity, P-δ curves, cracking, and failure modes between the FE and experimental findings were performed. Comparisons are presented in Table 6 and Figures 13 and 14. From Table 8, the model could predict well the failure modes of all experimentally tested RC beams without strengthening and those strengthened with jackets or with jackets and CFRP laminates (Figure 13). Moreover, the FE yield loads were predicted with an average error equal to 2.6 ± 0.64%, while the error in maximum load prediction was 2.2 ± 0.92% when compared with the experimental results (Table 8). Conversely, the FE model could predict well the P-δ curves with good agreement with the experimental ones in terms of stiffness and cracking propagation effects on increasing the beam deflections that occurred in the experimental curves for beams RB1 to RB3 (Figure 14b–d). The effect of bonding CFRP laminate to the bottom surface of the HSC jacket on increasing the beam stiffness and changing the failure characteristics was also adopted by the FE model (Figure 14e,f).

Table 8. Experimental and FE comparisons.

Beam ID	Experimental Results			FE Results			Comparisons	
	$P_{y,E.}$ (kN)	$P_{u,E.}$ (kN)	FM	$P_{y,FE}$ (kN)	$P_{u,FE}$ (kN)	FM	μ_y (%)	μ_u (%)
RB0	95.2	103.1	SH	96.7	105.4	SH	98.4	97.8
RB1	105.4	112.2	Ys	108.4	114.0	Ys	97.2	98.4
RB2	112.1	118.0	Ys	113.8	119.7	Ys	98.5	98.6
RB3	116.4	123.8	Ys	119.3	125.4	Ys	97.6	98.7
RB4	126.1	146.3	Ys, SH	130.0	150.7	Ys, SH	97.0	97.1
RB5	129.5	150.0	Ys, SH	133.9	156.4	Ys, SH	96.7	95.9
RB6	131.4	155.0	Ys, SH	134.5	158.5	Ys, SH	97.7	97.8
Mean							97.6	97.8
Standard deviation							0.64	0.92

$\mu_y = P_{y,E.}/P_{y,FE} \times 100$, $\mu_u = P_{u,E.}/P_{u,FE} \times 100$ and FM = failure mode.



(**a**) RB0

(**b**) RB1

(**c**) RB2

(**d**) RB3

(**e**) RB4

(**f**) RB5

(**g**) RB6

Figure 13. FE failure of the RC beams (the red color represents the developed cracks).

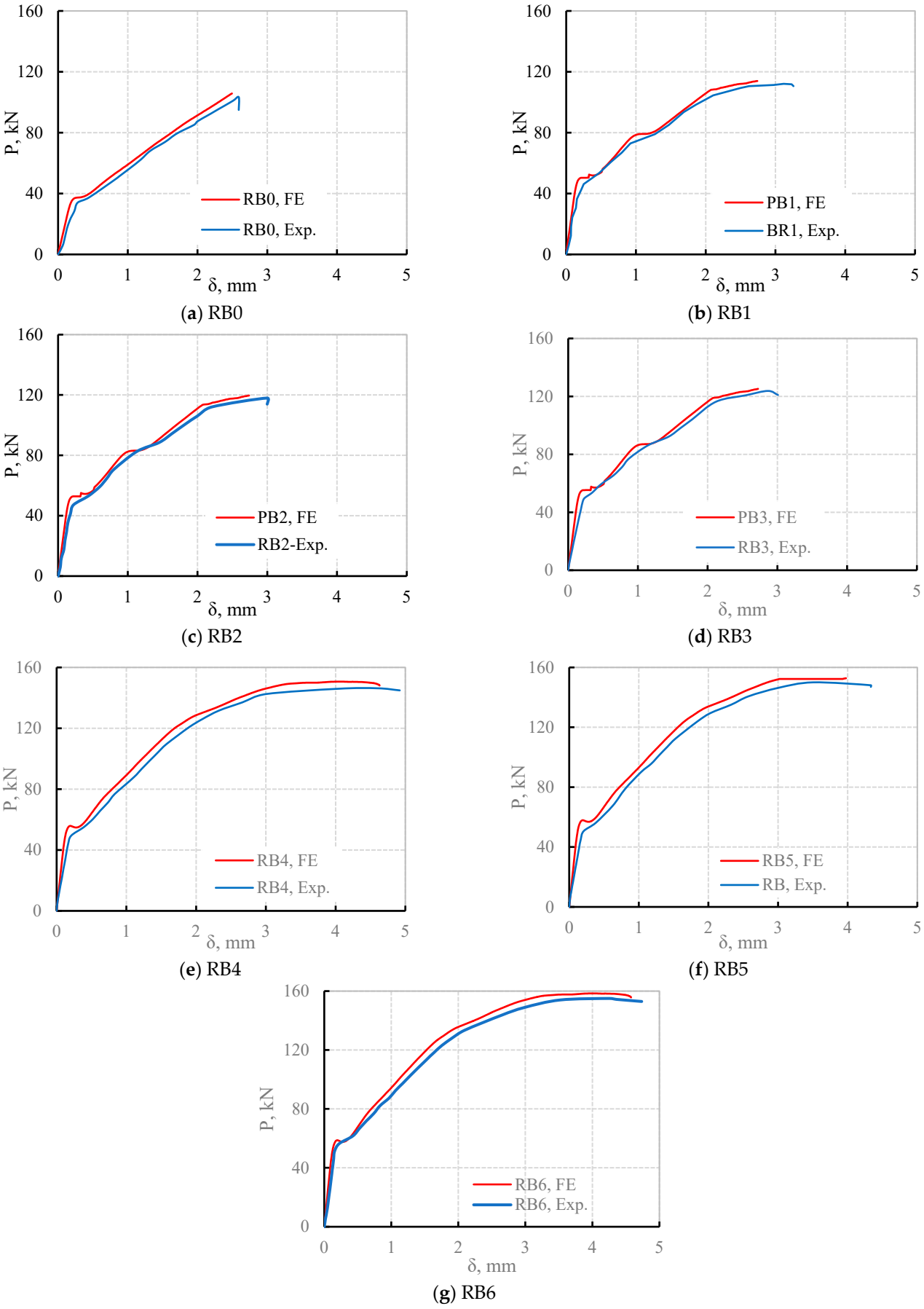
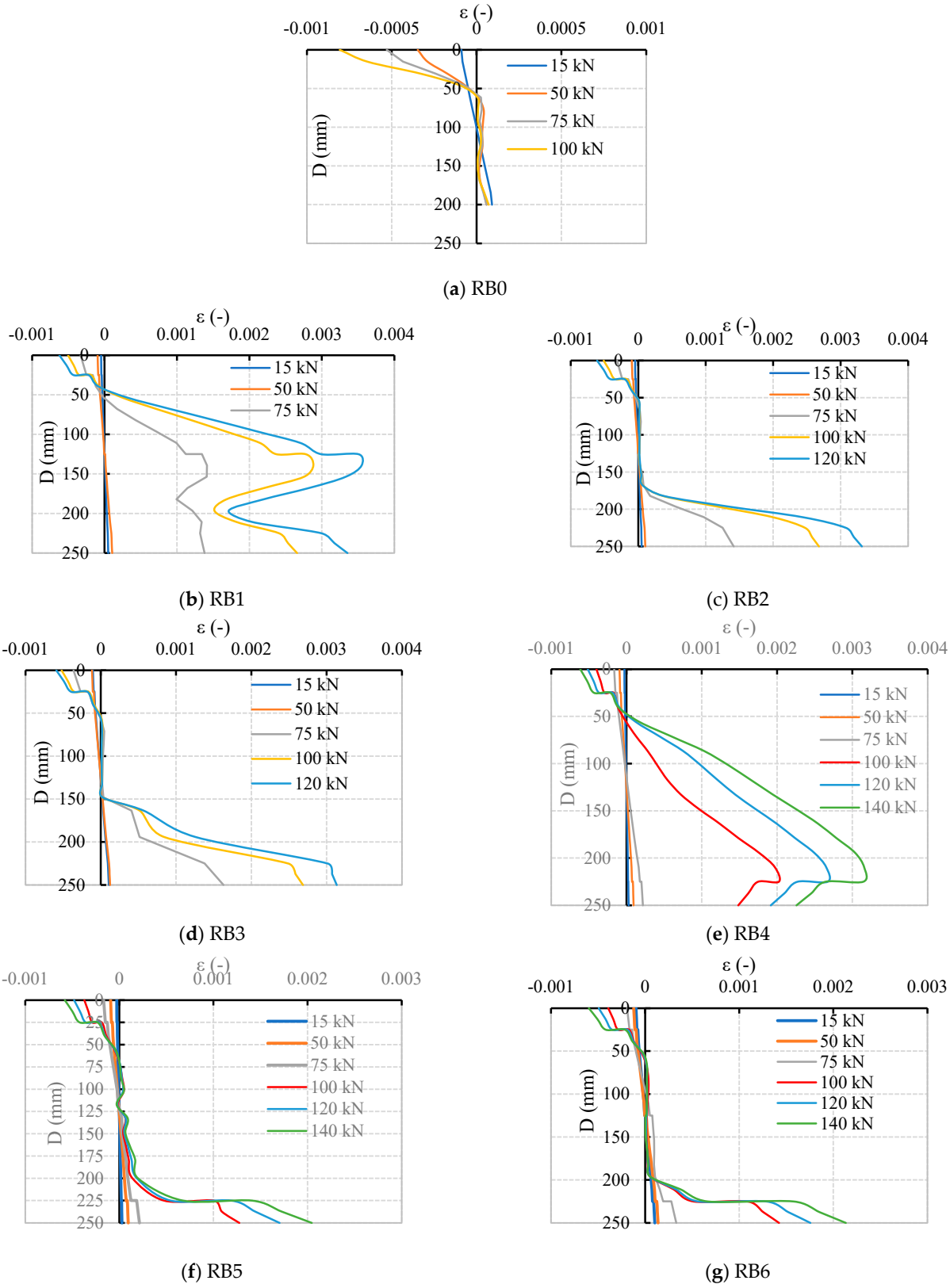


Figure 14. Experimental and FE comparisons for the tested beams.

4.4. Strain Profile Along the Beam Depth

For RB0, the strain profile was completely linear at load 15 kN, which means the RC beam section behaves as a homogenous material section as there was no cracking (the neutral beam axis lines are at the beam half-depth). As the load increased, the strain in tension was governed by steel as the concrete was cracked, while compression was linked to the concrete properties. The strain in the compression side increased with raising the load applied, but a slight increase in the tension side was observed (Figure 15a). As the beam fails due to shear before the steel yields, there was no obvious strain increment in the tension side like in the compression one (Figure 15a). Consequently, the strain profile for the three beams RB1 to RB3 was linear at loads 15 and 50 kN (Figure 15b). This ensured the beam carried most of the applied load through the concrete jacket having HSC properties. As the applied load increased for beam RB1, the strain increased in tension and compression due to tension concrete cracking (Figure 15b). As the concrete jacket cracked, the crack propagated rapidly through the beam depth (Figure 15b). For the two beams RB2 and RB3, the strain could propagate through the cracked concrete cover of the inner cracked beam, which means there was slippage between the strong concrete jacket (fcu = 72.8 and 74.6 MPa, respectively) and the weak inner section, and the applied load was resisted by the inner reinforced beam section and the outer HSC jacket and two separate sections at the middle of the beam (see Figure 15c,d). The strain profile of the three beams RB4 to RB6 followed the same one of the corresponding beams with HSC jacket strength RB1 to RB3, respectively, at low load levels. For the two beams RB5 and RB6, the drop in the tensile strain occurred at higher load levels than in the case of beams RB2 and RB3. This increment in the loading levels at which the tensile strain drop occurred was because of the bonded CFRP laminates delaying the bottom surface of the HSC jacket from forming cracks. Also, at the same load levels, the beams strengthened with HSC jackets showed nearly similar compressive strain values as the corresponding beams strengthened with HSC jackets and CFRP laminate; in contrast, they experienced higher tensile strain (Figure 15b–f). The RHS concrete affected the shape of the strain profile, as the tensile strength of the concrete jacket that was governed by the RSF content could control the initiation and propagation of the cracks for the strengthened beams. In the two beams RB1 and RB4, the relatively low strength of the concrete jacket compared to those of the other strengthened beams might allow more cracks to initiate in the tensile surface of the concrete jacket, which could affect the concrete and tensile steel bonding causing the distortion more than the strain profile compared to others beams. As the concrete jacket strength increased, the cracks propagated at the inner concrete beam and its jacket caused a drop in the strain profile for those beams at high loading levels (Figure 15). The strain finding assured the expected separation between the cracked beam and the HSC jacket caused the sudden failure and stopping of the machine loading.



(**a**) RB0

(**b**) RB1

(c) RB2

(**d**) RB3

(**e**) RB4

(**f**) RB5

(**g**) RB6

Figure 15. The stain profile along the beam depth at the beam middle section.

5. Conclusions

This research deals with the effect of adding the steel fibers extracted from used car tires (RSFs) to incorporate them as concrete components to obtain high-strength concrete (HSC). The HSC was used in this paper to strengthen pre-damaged beams by jacking.

In the first phase, twelve beams were subjected to an overload equal to 80% of their total expected bearing capacity to obtain damaged RC beams, while one beam was loaded to failure. In the second phase, the damaged beams were strengthened with HSC jacketing integrating RSFs with three contents (0, 0.25, and 0,5%) or by HSC jacking and bonding CFRP laminates to the bottom surface of the jacket. Moreover, the Abaqus finite element (FE) program was implemented to simulate the upgraded damaged beams. The following conclusions are drawn:

1. The HSC properties increased as the RSF % increased from 0 to 0.5%. As the RSF% increased from 0 to 0.25 and 0.5%, the average compressive strength of the HSC surged by 11.6% and 14.4%, respectively. In contrast, the tensile strength increased by 11.6 and 20.9, respectively.
2. The damaged beams' strength with the HSC jacket could experience higher load capacity than the unstrengthened beams depending on the RSC strength, which increased as the RSF content increased. As the RSF% was 0.25 and 0.5%, the load capacity of the damaged beams strengthened with the HSC jacket increased by 8.8, 14.5, and 20.1% over the unstrengthened beam.
3. Bonding the CFRP laminates to the bottom surface of the HSC jacket to strengthen the damaged RC beams increased the yield and maximum load capacity and stiffness of the RC beams compared to the corresponding beams strengthened with the HSC concrete jacket only. The load capacity of the beam strengthened with the HSC jacket and CFRP laminates increased by 41.0, 45.5, and 50.3% as the HSC jacket integrated 0, 0.25, and 0.5% RSF, respectively, compared to the unstrengthened beam.
4. The FE model could predict precisely the behavior of the damaged beams strengthened with HSC jackets and those strengthened with HSC jackets and CFRP laminate. The strain profile along the strengthened beam depth could clarify the effect of the RSF and CFRP laminates on the difference in the strengthened beams' behavior and failure modes.
5. The findings of this research would be beneficial in enhancing the behavior of precast concrete elements easily and could be used to enhance the capacity of old buildings suffering from cracking and return their appearance to the original one using this jacketing method using sustainable materials.

6. Future Work

Future work will focus on optimizing the long-term performance of beams strengthened with high-strength concrete (HSC) jackets integrated with recycled steel fibers (RSF), particularly by evaluating their fatigue resistance and the impact of environmental factors such as temperature and moisture. The authors also recommend exploring the use of hybrid fibers, combining RSF with other fiber types, to assess their effects on concrete properties and beam behavior. Additionally, the use of carbon fiber-reinforced polymer (CFRP) to reinforce the most stressed areas offers cost benefits, and future studies should examine the effectiveness of concrete jackets combined with limited lengths of CFRP sheets. The influence of beam size and loading conditions on the results should also be investigated to better understand their potential impact on the findings.

Author Contributions: Data curation, A.S.E., and A.E.-Z.; formal analysis, H.A.A., I.A.S., and A.S.E.; investigation, H.A.A.; methodology, H.A.A., I.A.S., and A.S.E.; resources, A.E.-Z.; software, H.A.A., I.A.S., and A.S.E.; validation, H.A.A., A.S.E., and A.E.-Z.; visualization, I.A.S.; writing—original draft, I.A.S.; writing—review and editing, A.E.-Z. All authors have read and agreed to the published version of the manuscript.

Funding: This research was funded by Taif University, Saudi Arabia, Project No. (TU-DSPP-2024-196).

Data Availability Statement: The data presented in this study are available on request from the corresponding author.

Acknowledgments: The authors extend their appreciation to Taif University, Saudi Arabia, for supporting this work through project number (TU-DSPP-2024-196).

Conflicts of Interest: The authors declare no conflicts of interest.

References

1. Kodsy, A.; Morcous, G. Predicting Strength of Non-Prestressed Concrete I-Beams Repaired/Strengthened in Flexure and Shear Using Ultra-High-Performance Concrete (UHPC). *Structures* **2023**, *58*, 105670. [CrossRef]
2. Nishino, M.; Aoki, T. Nonlinear Analysis and Damage Monitoring of a One-Sided Patch Repair with Delamination. *Compos. Struct.* **2006**, *73*, 423–431. [CrossRef]
3. Kim, T.-K.; Park, J.-S. Performance Evaluation of Concrete Structures Using Crack Repair Methods. *Sustainability* **2021**, *13*, 3217. [CrossRef]
4. Sharaky, I.A.; Selmy, S.A.I.; El-Attar, M.M.; Sallam, H.E.M. The Influence of Interaction between NSM and Internal Reinforcements on the Structural Behavior of Upgrading RC Beams. *Compos. Struct.* **2020**, *234*, 111751. [CrossRef]
5. Abdo, A.; Sharaky, I.A.; Ahmed, S. Shear Performance of Reinforced Concrete Beams Strengthened in Shear Using NSM Bars and Reinforced HSC Layers. *Struct. Concr.* **2023**, *24*, 7295–7313. [CrossRef]
6. Sharaky, I.A.A.; Torres, L.; Comas, J.; Barris, C. Flexural Response of Reinforced Concrete (RC) Beams Strengthened with near Surface Mounted (NSM) Fibre Reinforced Polymer (FRP) Bars. *Compos. Struct.* **2014**, *109*, 8–22. [CrossRef]
7. Reda, R.M.M.; Sharaky, I.A.A.; Ghanem, M.; Seleem, M.H.H.; Sallam, H.E.M.E.M. Flexural Behavior of RC Beams Strengthened by NSM GFRP Bars Having Different End Conditions. *Compos. Struct.* **2016**, *147*, 131–142. [CrossRef]
8. Zhang, S.S.; Yu, T.; Chen, G.M. Reinforced Concrete Beams Strengthened in Flexure with Near-Surface Mounted (NSM) CFRP Strips: Current Status and Research Needs. *Compos. Part B Eng.* **2017**, *131*, 30–42. [CrossRef]
9. Ahmed, S.; Sharaky, I.A.; Ibrahim, Y.E.; Abdo, A. Flexural Response of GFRP RC Beams Strengthened with Side and Bottom NSM GFRP Bars. *Case Stud. Constr. Mater.* **2023**, *18*, e01858. [CrossRef]
10. Megahed, F.A.; Seleem, M.H.; Badawy, A.A.M.; Sharaky, I.A. The Flexural Response of RC Beams Strengthened by EB/NSM Techniques Using FRP and Metal Materials: A State-of-the-Art Review. *Innov. Infrastruct. Solut.* **2023**, *8*, 289. [CrossRef]
11. Seleem, M.H.; Megahed, F.A.; Badawy, A.A.M.; Sharaky, I.A. Performance of NSM and EB Methods on the Flexural Capacity of the RC Beams Strengthened with Reinforced HSC Layers. *Structures* **2023**, *56*, 104950. [CrossRef]
12. Sharaky, I.A.; Elamary, A.S.; Alharthi, Y.M. Experimental and Numerical Investigation on the Flexural Performance of RC Slabs Strengthened with EB/NSM CFRP Reinforcement and Bonded Reinforced HSC Layers. *Eng. Struct.* **2023**, *289*, 116338. [CrossRef]
13. Tahmouresi, B.; Momeninejad, K.; Mohseni, E. Flexural Response of FRP-Strengthened Lightweight RC Beams: Hybrid Bond Efficiency of L-shape Ribbed Bars and NSM Technique. *Arch. Civ. Mech. Eng.* **2022**, *22*, 95. [CrossRef]
14. Hussain, A.M.; Sharif, I.B.M.; Baluch, G.J.A.-S. Flexural Behavior of Precracked Reinforced Concrete Beams Strengthened Externally by Steel Plates. *ACI Struct. J.* **1995**, *92*, 14–23. [CrossRef]
15. Wu, Y.-F.; Jiang, C. Quantification of Bond-Slip Relationship for Externally Bonded FRP-to-Concrete Joints. *J. Compos. Constr.* **2013**, *17*, 673–686. [CrossRef]
16. Alkhateeb, M.Y.; Hejazi, F. Reinforced Concrete Beams Externally Strengthened by CFRP Rods with Steel Plate, Anchorage Bolts, and Concrete Jacketing. *Structures* **2022**, *46*, 1994–2013. [CrossRef]
17. Ombres, L. Flexural Analysis of Reinforced Concrete Beams Strengthened with a Cement Based High Strength Composite Material. *Compos. Struct.* **2011**, *94*, 143–155. [CrossRef]
18. Brühwiler, E.; Denarié, E. Rehabilitation and Strengthening of Concrete Structures Using Ultra-High Performance Fibre Reinforced Concrete. *Struct. Eng. Int.* **2013**, *23*, 450–457. [CrossRef]
19. Kim, Y.Y.; Lee, B.Y.; Bang, J.W.; Han, B.C.; Feo, L.; Cho, C.G. Flexural Performance of Reinforced Concrete Beams Strengthened with Strain-Hardening Cementitious Composite and High Strength Reinforcing Steel Bar. *Compos. Part B Eng.* **2014**, *56*, 512–519. [CrossRef]
20. Abdullah, M.A.H.; Mohd Zahid, M.Z.A.; Ayob, A.; Muhamad, K. Flexural Behavior of Fire-Damaged Reinforced Concrete Beams Repaired with High-Strength Fiber Reinforced Mortar. *J. Struct. Fire Eng.* **2019**, *10*, 56–75. [CrossRef]
21. Alharthi, Y.M.; Emara, M.; Elamary, A.S.; Sharaky, I.A. Flexural Response and Load Capacity of Reinforced Concrete Beams Strengthened with Reinforced Mortar Layer. *Eng. Struct.* **2021**, *245*, 112884. [CrossRef]
22. Huang, Y.; Grünewald, S.; Schlangen, E.; Luković, M. Strengthening of Concrete Structures with Ultra High Performance Fiber Reinforced Concrete (UHPFRC): A Critical Review. *Constr. Build. Mater.* **2022**, *336*, 127398. [CrossRef]
23. Baggio, D.; Soudki, K.; Noël, M. Strengthening of Shear Critical RC Beams with Various FRP Systems. *Constr. Build. Mater.* **2014**, *66*, 634–644. [CrossRef]

24. Tahsiri, H.; Sedehi, O.; Khaloo, A.; Raisi, E.M. Experimental Study of RC Jacketed and CFRP Strengthened RC Beams. *Constr. Build. Mater.* **2015**, *95*, 476–485. [CrossRef]
25. Spadea, G.; Bencardino, F.; Sorrenti, F.; Swamy, R.N. Structural Effectiveness of FRP Materials in Strengthening RC Beams. *Eng. Struct.* **2015**, *99*, 631–641. [CrossRef]
26. Akbarzadeh, H.; Maghsoudi, A.A. Experimental and Analytical Investigation of Reinforced High Strength Concrete Continuous Beams Strengthened with Fiber Reinforced Polymer. *Mater. Des.* **2010**, *31*, 1130–1147. [CrossRef]
27. *Externally Bonded FRP Reinforcement for RC Structures, Technical Report Prepared by the Working Party EBR of Task Group 9.3*; Fib bulletin 14; International Federation of Structural Concrete: Lausanne, Switzerland, 2001.
28. Huang, Y.; Gu, D.; Mustafa, S.; Grünewald, S.; Luković, M. Shear Behaviour of Reinforced Concrete Beams Strengthened with Ultra-High Performance Fiber Reinforced Concrete (UHPFRC). *Case Stud. Constr. Mater.* **2023**, *19*, e02441. [CrossRef]
29. Etienot, S.; Xargay, H.; Ripani, M.; Caggiano, A.; Folino, P. Strengthening of Existing Reinforced Concrete Beams by Self Compacting Fiber Reinforced Concrete Jackets. *Constr. Build. Mater.* **2024**, *448*, 138233. [CrossRef]
30. Folino, P.; Etienot, S.; Ripani, M.; Xargay, H. Shear Strengthening of Existing Concrete Beams Using Fiber Reinforced Concrete. *Procedia Struct. Integr.* **2024**, *64*, 1452–1459. [CrossRef]
31. Luu, X.-B. Finite Element Modelling of Reinforced Concrete Beam Strengthening Using Ultra-High Performance Fiber-Reinforced Shotcrete Combined with Reinforcing Bars. *Structures* **2024**, *60*, 105794. [CrossRef]
32. Yoo, D.Y.; Oh, T.; Choi, J.; Min, K.H.; Shin, H.O. Structural Strengthening of Reinforced Concrete Beams Using Ultra-High-Performance Concrete with Various Fiber Volume Fractions and Layer Thicknesses. *Structures* **2024**, *70*, 107735. [CrossRef]
33. Iqbal, S.; Ali, A.; Holschemacher, K.; Bier, T.A.; Shah, A.A. Strengthening of RC Beams Using Steel Fiber Reinforced High Strength Lightweight Self-Compacting Concrete (SHLSCC) and Their Strength Predictions. *Mater. Des.* **2016**, *100*, 37–46. [CrossRef]
34. Noshiravani, T.; Brühwiler, E. Analytical Model for Predicting Response and Flexure-Shear Resistance of Composite Beams Combining Reinforced Ultrahigh Performance Fiber-Reinforced Concrete and Reinforced Concrete. *J. Struct. Eng.* **2014**, *140*, 04014012. [CrossRef]
35. Shirai, K.; Yin, H.; Teo, W. Flexural Capacity Prediction of Composite RC Members Strengthened with UHPC Based on Existing Design Models. *Structures* **2020**, *23*, 44–55. [CrossRef]
36. Zeng, J.J.; Zeng, W.B.; Ye, Y.Y.; Liao, J.J.; Zhuge, Y.; Fan, T.H. Flexural Behavior of FRP Grid Reinforced Ultra-High-Performance Concrete Composite Plates with Different Types of Fibers. *Eng. Struct.* **2022**, *272*, 24–26. [CrossRef]
37. Yan, Z.; Zeng, J.J.; Zhuge, Y.; Liao, J.J.; Zhou, J.K.; Ma, G. Compressive Behavior of FRP-Confined 3D Printed Ultra-High Performance Concrete Cylinders. *J. Build. Eng.* **2024**, *83*, 108304. [CrossRef]
38. Rabehi, B.; Ghernouti, Y.; Li, A.; Boumchedda, K. Comparative Behavior under Compression of Concrete Columns Repaired by Fiber Reinforced Polymer (FRP) Jacketing and Ultra High-Performance Fiber Reinforced Concrete (UHPFRC). *J. Adhes. Sci. Technol.* **2014**, *28*, 2327–2346. [CrossRef]
39. El Maaddawy, T.; El Sayed, M.; Abdel-Magid, B. The Effects of Cross-Sectional Shape and Loading Condition on Performance of Reinforced Concrete Members Confined with Carbon Fiber-Reinforced Polymers. *Mater. Des.* **2010**, *31*, 2330–2341. [CrossRef]
40. Tayeh, B.A.; Naja, M.A.; Shihada, S.; Arafa, M. Repairing and Strengthening of Damaged RC Columns Using Thin Concrete Jacketing. *Adv. Civ. Eng.* **2019**, *2019*, 2987412. [CrossRef]
41. Zhang, Z.; Hsu, C.-T.T. Shear Strengthening of Reinforced Concrete Beams Using Carbon-Fiber-Reinforced Polymer Laminates. *J. Compos. Constr.* **2005**, *9*, 158–169. [CrossRef]
42. Ahmed, S.; Sharaky, I.A.; El Sayed, S.; Hassan, H.; Abdo, A. Effect of Rubberized Concrete Integrating Uncoated and Coated Crumb Rubber on the Flexural Behavior of the RC Beams Reinforced with Steel and GFRP Bars. *Constr. Build. Mater.* **2024**, *426*, 136192. [CrossRef]
43. Najim, K.B.; Hall, M.R. Mechanical and Dynamic Properties of Self-Compacting Crumb Rubber Modified Concrete. *Constr. Build. Mater.* **2012**, *27*, 521–530. [CrossRef]
44. Gesolu, M.; Güneyisi, E. Permeability Properties of Self-Compacting Rubberized Concretes. *Constr. Build. Mater.* **2011**, *25*, 3319–3326. [CrossRef]
45. *BS EN 12390-22009*; BSI Testing Hardened Concrete—Part 2: Making and Curing Specimens for Strength Tests. British Standards Institution: London, UK, 2009.
46. *ASTM C39-05*; Standard Test Method for Compressive Strength of Cylindrical Concrete Specimens. ASTM International: West Conshohocken, PA, USA, 2008.
47. Shen, J.; Dai, H.; Zhou, G.; Shi, J. Shear Behavior of Pre-Damaged RC Beams Strengthened with UHPFRC-CFRP Grid Layer. *Compos. Struct.* **2024**, *349–350*, 118520. [CrossRef]
48. Tan, C.; Sun, T.; Zhao, H.; Tu, L.; Qiao, D.; Shao, X. Shear Behavior of Pre-Damaged RC Beams Strengthened with Steel Plate and UHPC. *J. Constr. Steel Res.* **2024**, *212*, 108287. [CrossRef]
49. Pereiro-Barceló, J.; Lenz, E.; Torres, B.; Estevan, L. Mechanical Properties of Recycled Aggregate Concrete Reinforced with Conventional and Recycled Steel Fibers and Exposed to High Temperatures. *Constr. Build. Mater.* **2024**, *452*, 138976. [CrossRef]

50. Wang, Z.; Liang, X.; Wan, S.; Cao, Z.; Weng, S.; Wu, K. Experimental and Theoretical Investigation on Axial Tensile Behavior of Ultra-High Performance Concrete (UHPC) with Recycled Steel Fibers from Waste Tires. *Constr. Build. Mater.* **2024**, *456*, 139300. [CrossRef]
51. Kordina, K.R.; Mancini, G.; Schäfer, K.; Schieβl, A.; Zilch, K. *Fib Bulletin 54. Structural Concrete Textbook on Behaviour, Design and Performance Second Edition Volume 4*; Balázs, G.L., Ed.; The International Federation for Structural Concrete: Lausanne, Switzerland, 2010; ISBN 9782883940949.
52. Carreira, D.J.; Kuang-Han, C. Stress-Strain Relatonship for Reinforced Concrete in Compression. *ACI Struct. J.* **1985**, *83*, 797–804. [CrossRef]
53. Aslani, F.; Jowkarmeimandi, R. Stress-Strain Model for Concrete under Cyclic Loading. *Mag. Concr. Res.* **2012**, *64*, 673–685. [CrossRef]
54. Wosatko, A.; Genikomsou, A.; Pamin, J.; Polak, M.A.; Winnicki, A. Examination of Two Regularized Damage-Plasticity Models for Concrete with Regard to Crack Closing. *Eng. Fract. Mech.* **2018**, *194*, 190–211. [CrossRef]

Disclaimer/Publisher's Note: The statements, opinions and data contained in all publications are solely those of the individual author(s) and contributor(s) and not of MDPI and/or the editor(s). MDPI and/or the editor(s) disclaim responsibility for any injury to people or property resulting from any ideas, methods, instructions or products referred to in the content.